COMPARISON OF REPROCESSED ASAR WM OCEAN WAVE SPECTRA WITH WAM AND BUOY SPECTRA

H. Johnsen [(1)], **F. Collard** [(2)]

(1) Norut IT, Postboks 6434, Forskningsparken, 9294 Tromsø, Norway, e-mail: harald.johnsen@itek.norut.no
(2) BOOST Technologies, 115 rue Claude Chappe,29280 Plouzané, France, e-mail: fabrice.collard@boost-technologies.com

ABSTRACT

A major upgrade of the processing of Envisat ASAR Wave Mode (WM) products has been done followed by an extensive geophysical validation. The calibration/validation of the products are conducted using collocated WAM model as provided by ECMWF as well as available buoy data. Validation shows a significant improvement in the geophysical quality of the both the Level 1 WVS and the Level 2 WVW product. Less RMS deviation and bias between WVW and WAM or buoy wave spectra parameters are observed. We observe that the RMS error of H_s^{12} and T_p^{12} of the WVW is similar to values of WAM, both compared to the buoys. For the bias, the WVW values are slightly higher than the WAM values, both compared to buoy. For H_s^{12} these are RMS=0.57m (0.52m) and BIAS=0.20m (0.07m), and for T_p^{12} these are RMS=1.03s (1.13s) and BIAS=-0.25s (0.03s), where the values in the brackets are corresponding WAM values.

1. INTRODUCTION

Based on the results of systematic long term validation (from launch until end of 2005) of the ASAR WM products (WVS, WVW) [1],[2], a major upgrade of the WM processing algorithms was developed and implemented. The major problems observed in the first version of the WM Level 2 algorithm are related to; - large number of non-physical spectra, - overestimation of mean period of swell, - overestimation of Hs, especially at low sea-state, - ambiguity in swell propagation direction at low SNR, - azimuth cut-off value.

The solutions were found by; - detrending in spectral domain, - modification of the modulation transfer function (MTF) at low wavenumbers, - improved SNR measure, -new ambiguity flag, - and a new azimuth cut-off estimator. The main upgrades are outlined and examplified in this paper. The upgraded alogrithms have been extensively validated using collocated WAM and buoy spectra. The geophysical validation consist of systematic regional comparison with collocated wave parameters of the WAM as well as buoy data, whenever available. Validation shows in general a significant improvement in the geophysical quality of the both the WVS and the WVW product.

We also observe that much more of the WM data gives meaningful wave spectra (especially in coastal areas), and an improved flagging of ambiguity data is achieved as well as the number of products passing the quality control. The latter is of importance for the assimilation of WVW products into NWP models. We also observed individual cases where we clearly see how WVW spectra add consistently new information to the swell part of the WAM spectra.

The reprocessing of the global Envisat ASAR WM data archive is undertaken at IFREMER using the upgraded WM algorithms. The near real-time processing of WM products at the Envisat Ground Segment will in near future also be upgraded with the new algorithm.

The reprocessed ocean wave spectra have also been used to illustrate swell tracking capabilities in the Pacific ocean using ASAR WM data. This can be used to improve the swell forcast in the Pacific coast of US and South-America.

2. ALGORITHM UPGRADE

The major upgrades of the Level 2 algorithm (i.e. the WVW processing) were the improvements of the detrending of the data, - the modification of the modulation transfer function (MTF), - a new ambiguity flag measure, - and improvements of azimuth cut-off estimator. In the following we briefly describe and illustrate the improvements.

Proc. 'Envisat Symposium 2007', Montreux, Switzerland
23–27 April 2007 (ESA SP-636, July 2007)

2.1 Detrending

The large number of non-physical specta was maily related to improper detrending of the imagette, previously only done in the spatial domain. An additional non wave feature removal was applied in the Fourrier domain of the image cross spectra by removing spectral contributions that are maximum at the cutoff frequencies (800m) and decreasing monotonically to higher wavenumbers.

2.2 Modulation transfer function

It has further been observed that the actual SAR MTF tends to overestimate the swell at low wavenumbers. This has the double impact of reducing the relative importance of rather developed wind seas (in the range 100-200m) and overestimating the wavelength of swell systems. This artefact is due to the assumption that all spectral components of the wave spectrum are free propagating waves. This assumption is no longer valid for wavenumber lower than the spectral peak, which are not propagating waves but effects of wave groupiness (limited number of waves within a group equivalent to a peak broadening in the spectral domain). We thus apply, on wavenumber lower than the peak for each single direction, the same transfer function as for the peak wavenumber.

2.3 Propagation ambiguity

The wave propagation ambiguity removal in the Level 2 processing is based on generating a symmetric and a anti-symmetric wave spectra by applying the MTF on the real and imaginary parts of the cross-spectra, respectively. Then only those wave components in the symmetric spectrum with values above certain positive value in the anti-symmetric spectra are kept. However, it has turned out that the imaginary part of the cross-spectra has often a low SNR, which in combination with the MTF may produce ambiguities in the wave direction retrievals. We thus decided to apply on the imaginary part of the cross-spectra a modified MTF that is thresholded to avoid noise amplification at low frequencies and a weighting function based on the ambiguous inverted wave spectrum. This improvement in ambiguity removal has a strong impact when several wave systems are present at the ocean surface since the imaginary part of the longer wave system might have an SNR lower than the surrounding low frequencies or noise contribution. Additionally, a new parameter (*ambFac*) is used to assess the confidence flag of the swell inversion.

2.4 Azimuth cut-off length

The estimation of the azimuth cut-off wavelength, λ_{cut} is based on using a Gaussian roll-off function for the azimuth profile of the cross-correlation function. The iterative procedure for doing the minimization is now based on the bisection algorithm, which is observed to perform better than the previous Newton iteration scheme.

3. GEOPHYSICAL VALIDATION

3.1 Validation methodology and data

The validation consists of intercomparison of wave spectral parameters derived from the various sources (ASAR, NDBC buoys, WAM), followed by an estimation of RMS error and bias. The wave spectral parameters of particular interest is the wave period, T_p, the significant waveheight, H_s, and the wave direction, Φ_p, which are derived from the two-dimensional wave spectra as described in the following. Example of collocated two-dimensional wave spectra is shown in Fig.1.

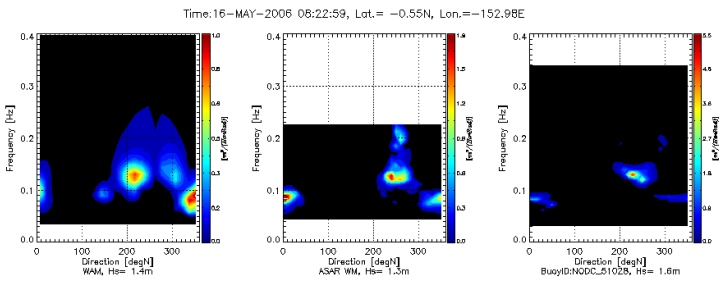

Figure 1. Collocated ocean wave spectra from WAM (left), ASAR WM (mid), and buoy (right).

The ASAR Wave Mode Level 2 spectra (WVW product) are given on log-polar grid in wavenumber and direction domain, $F(k,\varphi)$. Note that the ASAR spectrum is in general not the total ocean wave spectrum, but only the wave spectrum within the SAR imaging domain. The size of this domain is again

dependent on the azimuth cut-off which again is dependent on the sea state. The frequency-, $F(f)$ and directional spectra, $\psi(\varphi)$ are then derived from the Level 2 spectra, $F(k,\varphi)$ according to the formulas of Eqs. 1 - 6:

$$(1) \quad F(f) = \int F(k,\varphi) k \cdot dkdf \cdot d\varphi$$

$$(2) \quad \psi(\varphi) = \int F(k,\varphi) dk$$

$$(3) \quad \phi(f) = \tan^{-1}\left(\frac{\int F(k,\varphi)\sin\varphi d\varphi}{\int F(k,\varphi)\cos\varphi d\varphi} \right)$$

where $dkdf = 4\pi\sqrt{k/g}$. The significant waveheights, H_s, H_s^{12} mean periods, T_p, T_p^{12}, and mean wave direction, Φ are then computed as:

$$(4) \quad H_s = 4\sqrt{\int_{f_{\min}}^{f_{\max}} F(f)df}, \qquad H_s^{12} = 4\sqrt{\int_{f_{\min}}^{1/12} F(f)df}$$

$$(5) \quad T_p = \frac{\int_{f_{\min}}^{f_{\max}} F(f) f^{-1} df}{\int_{f_{\min}}^{f_{\max}} F(f)df}, \quad T_p^{12} = \frac{\int_{f_{\min}}^{1/12} F(f) f^{-1} df}{\int_{f_{\min}}^{1/12} F(f)df}$$

$$(6) \quad \Phi = \tan^{-1}\left(\frac{\int_{f_{\min}}^{f_{\max}} F(f)\sin(\phi(f))df}{\int_{f_{\min}}^{f_{\max}} F(f)\cos(\phi(f))df} \right)$$

where $f_{\min}, f_{\max}$ are the lowest and highest frequencies in the spectrum to be computed over. Similar parameters can be derived from the co-located WAM and buoy spectra. Spectral peak period, T_{peak} and direction, Φ_{peak}, given as the peak of $F(f)$ and $\psi(\varphi)$, respectively, are also computed and compared. The wave directions are always clock-wise from north towards the direction the waves propagate. The H_s^{12}, Φ^{12} and T_p^{12} are computed for waves with period longer than 12 sec, which in most cases are longer than then the azimuth cut-off period, $T_{cut} = 2\pi\lambda_{cut}/g$.

A partitioning scheme has also been used in the validation of the WAM and ASAR wave spectra for comparison of the swell parameters.

3.2 Validation results

Quality Control:

There are several parameters within the WVW product that can be used to assess the quality of the spectra. One important parameter is the ambiguity parameter that can be used to filter out wave spectra with low signal-to-noise ratio in the imaginary part of the input image cross-spectra. In Fig.2 we show the $\sqrt{\text{ambFac}}$ as function of swell wave direction difference between the WVW and the WAM spectra.

Fig.2 shows that the swell wave direction difference between WAM and WVW spectra increases with decreasing ambiguity factor, and that a suitable threshold to use is $\sqrt{\text{ambFac}} \approx 3$ for removing corrupted spectra. In Fig.3 we show the impact on the histogram of the swell wave direction difference when using $\sqrt{\text{ambFac}} \approx 0$ and $\sqrt{\text{ambFac}} \approx 3$.

Fig.3 shows that by filtering the data using the *ambFac* reduces the RMS error from 40° to 28°. We also see that the reduction of the RMS error comes from removing the 180° side lobes of the histogram and sligthly shrinking the main lobe. The filtering of the data with $\sqrt{\text{ambFac}} > 3$ reduces the amount of data used by 30%. The validation shown in the following is based on using the above filtering of the data.

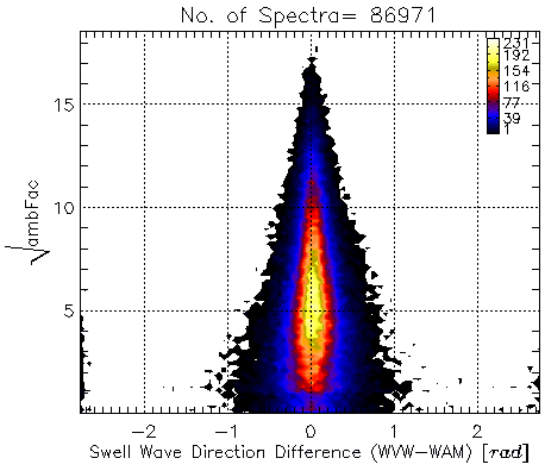

Figure 2. The square root of WVW ambiguity parameter as function of the difference between the WVW and the WAM swell wave directions.

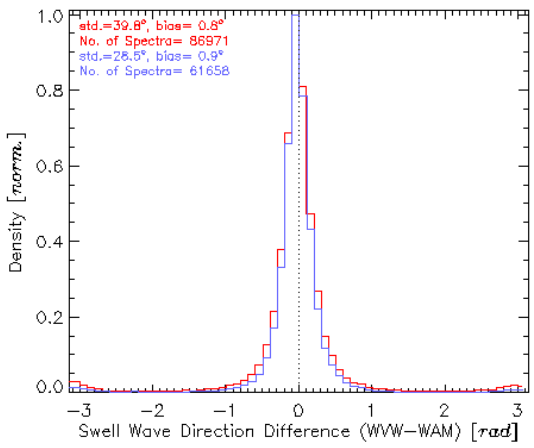

Figure 3. Histogram of swell wave direction difference between WVW and WAM spectra with $\sqrt{\text{ambFac}} > 0$ *(red) and* $\sqrt{\text{ambFac}} > 3$ *(blue).*

Significant Waveheight:

In the Fig.4 – 6 we show the waveheight difference, ΔH_s and ΔH_s^{12}, between WAM and WVW, between WAM and buoy, and between WVW and buoy. The triple collocated data are from US coast of Atlantic, Mexico Gulf, US Pacific Coast , Hawaii, and Christmas Island, while the collocated WVW and WAM data are globally distributed. In Fig.4 we show the histogram of ΔH_s and ΔH_s^{12} from WVW and WAM. The data set consist of 61658 spectra, acquired globally.

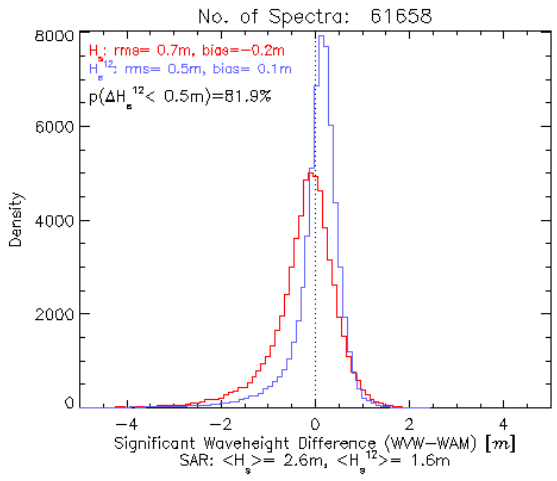

Figure 4. Histogram of significant waveheight differences (ΔH_s *and* ΔH_s^{12}*) between WVW and WAM spectra achieved globally using 61658 spectra from each sensor.*

The skewness of the histogram of H_s in Fig.4 comes from the azimuth cut-off effect tending to reduce the energy of the WVW spectra at high azimuth wavenumbers. For H_s^{12} this effect is significantly reduced. Fig.4 shows that ΔH_s^{12} has a RMS error of 0.5m and a bias of 0.1m. We also see that 82 % of the WVW spectra has a $\Delta H_s^{12} \le 0.5\text{m}$. We also see from Fig. 5 that the dependency of ΔH_s^{12} on the wind speed is weak.

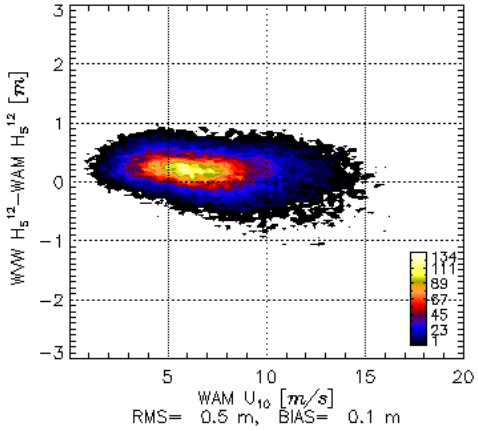

Figure 5. ΔH_s^{12} *from WVW and WAM spectra as function of WAM wind speed.*

In Fig.6 we do the same comparison, but now using the triple collocated data set. We see that for H_s^{12} the RMS error and bias between SAR and buoy is 0.6m and 0.2m, respectively, while between WAM and buoy they are 0.5m and 0.1m. The corresponding SAR and WAM values are 0.4m and 0.1m.

We conclude that the WVW product is able to provide a reasonable good estimate of the significant waveheight for waves with period longer than 12 sec (prob{ $\Delta H_s^{12} \le 0.5\text{m}$ } = 82%).

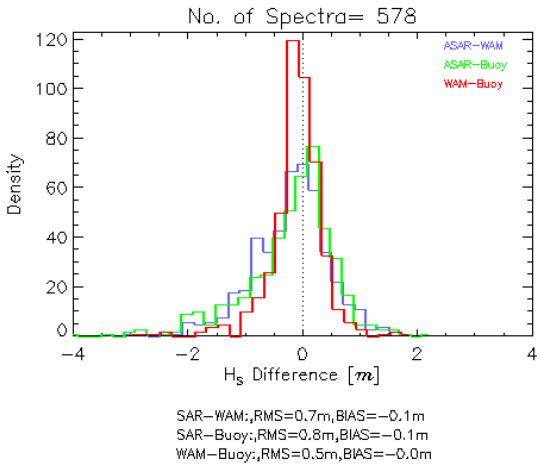

a)

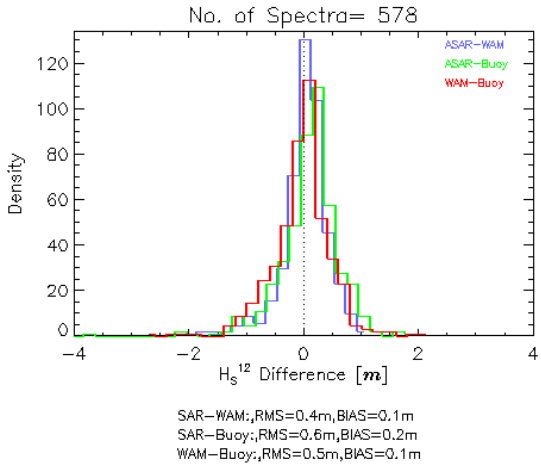

b)

Figure 6. Histogram of significant waveheight difference between WAM, WVW and buoy spectra using 578 spectra from each sensor.

Mean Period:

The difference in mean periods, ΔT_p and ΔT_p^{12} between WVW and WAM are shown in Fig.7 and in Fig.8 we show the same using the triple collocated data set of WAM, WVW and buoy spectra. We see that for T_p^{12} the RMS error and bias between SAR and buoy is 1.0s and -0.3s, respectively, while between WAM and buoy they are 1.1s and 0.0s. The corresponding SAR and WAM values are 0.6s and -0.3s, both from the global and the triple collocated data set. We conclude that there is very small differences in the mean wave periods between WAM and WVW as compared to buoy i.e. (prob{ $T_p^{12} \leq 0.6s$ } = 69%).

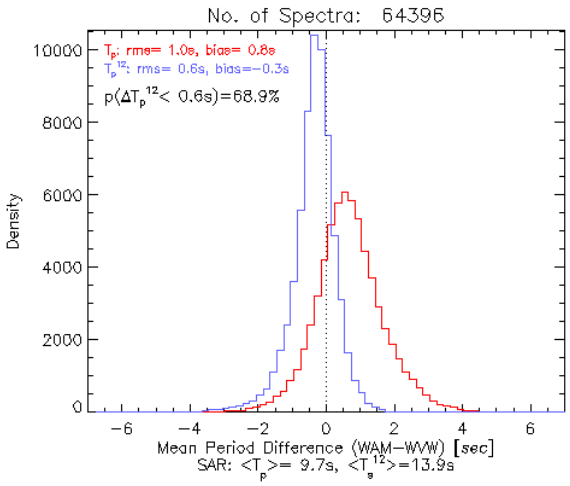

Figure 7. Histogram of mean period differences (ΔT_p and ΔT_p^{12}) between WVW and WAM.

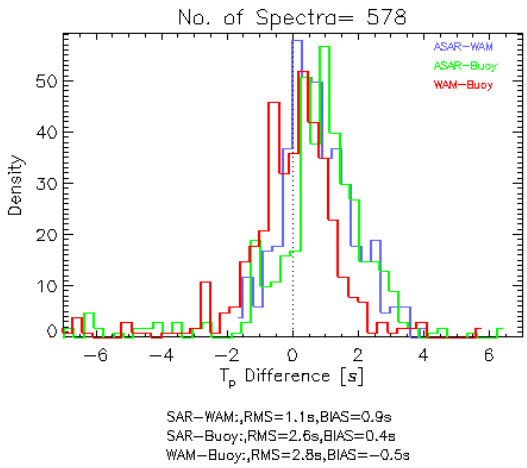

a)

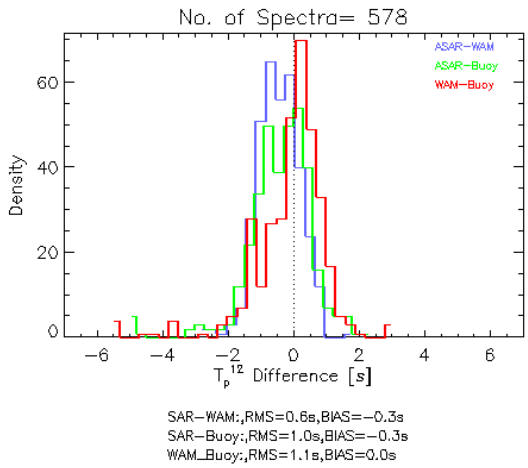

b)

Figure 8. Histograms of mean period differences a) ΔT_p and b) ΔT_p^{12} between WAM, WVW and buoy

spectra using 578 spectra from each sensor.

Mean Wave Direction:

The directional informations from the available buoy data is limited, so the wave direction comparison is based on the global WVW and WAM collocated data set. In Fig.9 we show the histograms of mean wave direction differences $\Delta\phi$ and $\Delta\phi^{12}$, and in Fig.10 the swell wave direction, $\Delta\phi_{swell}$ and the peak wave directions, $\Delta\phi_{peak}$, $\Delta\Phi^{12}_{peak}$.

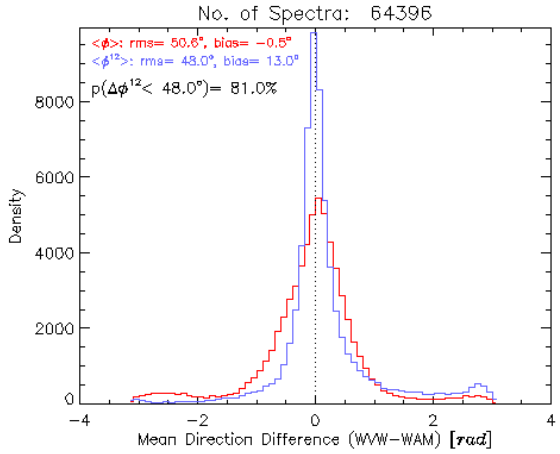

Figure 9. Histograms of mean wave direction differences ($\Delta\phi$ and $\Delta\phi^{12}$) between WVW and WAM.

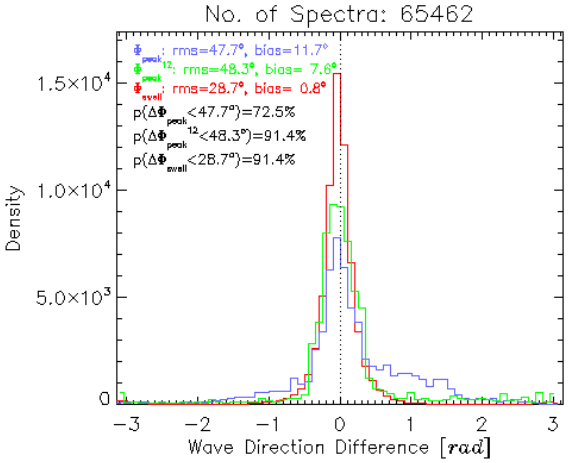

Figure 10Histograms of peak wave direction differences $\Delta\Phi_{peak}$ (blue), $\Delta\Phi^{12}_{peak}$ (green), and swell wave direction difference $\Delta\Phi_{swell}$ (red).

For $\Delta\phi^{12}$ we observe an RMS error of 47.5° and a bias of 12.4°, with 81% of the data is within this error bound (prob{ $\Delta\phi^{12}$ <47.5° } = 81%).

From Fig.10 we get for the peak wave direction an RMS error of 47° and a bias of 11°, while for the swell the values are 28° and 0.8°. We also observe that the deviation in swell wave direction between WAM and WVW spectra are less than 28° in 91% of the cases.

Wind Speed:

An estimate of the local wind speed is also stored within the WVW product, based on using the CMOD-IF2 backscatter model and assuming a wind direction of 45°. The scatterplot of WVW versus WAM wind speed is shown in Fig.11.

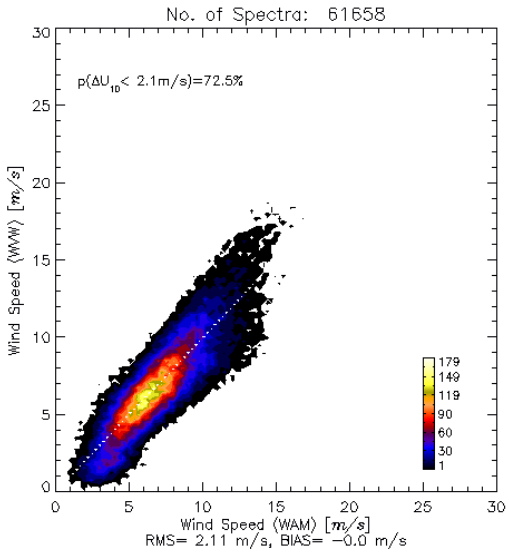

Figure 11. Scatter plot of WVW versus WAM wind speed achieved globally.

4. SUMMARY

We conclude that the WVW product is able to provide a reasonable good estimate of key wave spectra parameters for the long wavelength part of the spectra ($\lambda < \lambda_{cut}$). For the significant waveheight for waves with period longer than 12 sec we achieve a prob{ $\Delta H_s^{12} \le 0.5$m } = 82%. For the mean period we conclude that there is very small differences in the mean wave periods between WAM and WVW as compared to buoy with a prob{ $\Delta T_p^{12} \le 0.6$s } = 69%. For the mean

wave direction we achieve a prob{ $\Delta\phi^{12} \leq 48^{o}$ } = 81%. Similar values are achieved for the peak period and direction as shown in Table 1. The overall percentage of WVW spectra passing the quality control is on global basis 71%. This is of importance for the assimilation of WVW products into NWP models. A summary of the validation results is presented in Table1.

Table 1. Summary of validation of SAR wave spectral parameters against WAM and buoy. The values in the parenthesis are from the WAM versus buoy comparison.

SAR	WAM		BUOY	
	std	bias	std	bias
H_s	0.70m	-0.18m	0.84m (0.51m)	-0.12m (0.00m)
H_s^{12}	0.54m	0.08m	0.57m (0.52m)	0.20m (0.07m)
H_{swell}	0.90	-0.22		
T_p	0.98s	0.79s	2.56s (2.76s)	0.44s (-0.47s)
T_p^{12}	0.64s	-0.25s	1.03s (1.13s)	-0.25s (0.04s)
T_{peak}	1.74s	0.07s	2.11s (2.43s)	0.73 (0.51s)
T_{swell}	2.13s	-1.09		
Φ	50.5°	-0.85°		
Φ_{12}	47.5°	12.39°		
Φ_{peak}	47.71°	11.10°		
Φ_{peak}^{12}	48.60°	7.70°		
Φ_{swell}	28.44°	0.91°		
U_{10}	2.10m/s	0.00m/s	2.92m/s (2.38m/s)	0.22m/s (0.51m/s)

ACKNOWLEDGEMENT:

The work was co-funded by ESA/ESRIN Contract No. 17376/03/I-OL, and Norges forskningsråd Contract No. 153781. We acknowledge the use of the collocated data from CERSAT, at IFREMER, Plouzané (France).

REFERENCES

1. Kerbaol V., Johnsen H., Chapron B., Rosich B., "Quality assessment of ASAR Wave Mode products based on regional and seasonal comparison with WAM model output", ERS/Envisat Symposium, 6-10 Sept. 2004, Salzburg
2. Johnsen H., Engen G., Chapron B., "Validation of ASAR Wave Mode Level 2 product using WAM and buoy spectra", Proceeding Coastal & Marine Applications of SAR, 8-12 Sept., 2003, Svalbard, ESA SP-565.